ACS Biomaterials SCIENCE & ENGINEERING
Article
Cite This: ACS Biomater. Sci. Eng. 2018, 4, 1609−1621

Enhanced Mechanical and Biological Performance of an Extremely Fine Nanograined 316L Stainless Steel Cell−Substrate Interface Fabricated by Ultrasonic Shot Peening

Fei Yin,*[,†,‡] Rong Xu,[‡,§] Shan Hu,[†] Kejie Zhao,[‡,§] Shiqi Yang,[∥] Shihuan Kuang,[∥] Qiang Li,[⊥] and Qingyou Han*[,†,‡]

[†]School of Engineering Technology, [‡]Brick Nanotechnology Center, [§]School of Mechanical Engineering, [∥]Department of Animal Sciences, and [⊥]School of Materials Engineering, Purdue University, West Lafayette, Indiana 47907, United States

ABSTRACT: An extremely fine nanograined (NG) rough surface with the average grain size of 10 nm was successfully fabricated on 316L stainless steel (316L SS), which is a commonly used bioimplant metallic materials, via a simple physical therapy, namely, ultrasonic shot peening (USP). This extremely fine NG rough surface was proposed as the cell−substrate interface to enhance the mechanical and biological performance of 316L SS in orthopedic applications. Nanoindentation and micropillar compression tests indicated the significant improvement of the nanohardness and yield strength of the developed NG-316L SS, respectively, and the "in vitro" studies demonstrated that the developed extremely fine NG-316L SS rough surface could significantly enhance the attachment of the human osteoblast cells (Saos-2) compared with the as-received coarse-grained 316L SS surface. The observed mechanical and biological enhancement of the extremely fine NG-316L SS surface can be attributed to the ultrahigh-density nanosized grain boundaries, which could obstruct dislocation movement when the materials undergo plastic deformation and promote protein adsorption by providing a continuum of probable binding sites with partial surface coverage when the material encounters biological environments. In addition, aggregated protein particles were clearly observed on the proposed extremely fine NG-316L SS surface when it was used for the substrate of the human osteoblast cells. The findings and the advanced surface engineering technology utilized in this paper could promote the currently proposed concept that using nanograined/ultrafine grained cell−substrate interface for mechanical and biological enhancement of bioimplant materials from the current practice level of "hundreds of nanometers" to that of "tens of nanometers" or possibly even "several nanometers".

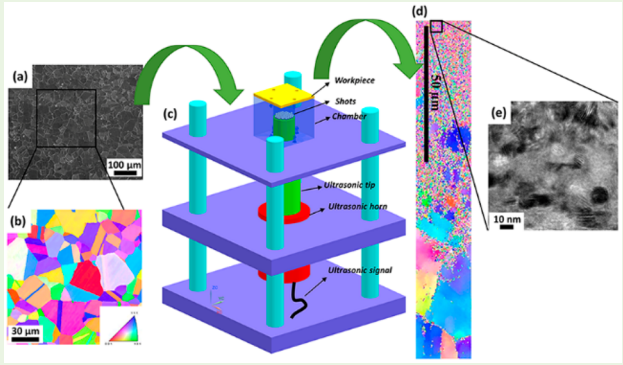

KEYWORDS: *extremely fine nanograined cell−substrate interface, ultrasonic shot peening, nanohardness, micropillar compression, human osteoblast cell*

1. INTRODUCTION

Requirements of the next generation bioimplant materials include long-term durability and fast osseointegration.[1] It was acknowledged that cells could respond to the nanograined/ultrafine-grained surface because "in vivo" they are living in an environment of the nanofeatures, and nanograined surfaces were considered to have the potential to alter adsorption of proteins that could mediate cell adhesion and enhance subsequent tissue growth.[2−5] Recently, applications of the nanograined (NG)/ultrafine-grained (UFG) cell−substrate interface for the enhancement of mechanical and biological performance of the bioimplant materials have drawn more and more attention from the research communities of materials science and bioengineering worldwide.[6−8]

Bahl et al. pointed out that the nanostructured metals are an ideal class of biomaterials for application in orthopedics because they can improve the mechanical performance and biological response of the biomedical implants. They developed a NG surface layer on the 316L stainless steel (316L SS) by using surface mechanical attrition treatment (SMAT) and observed a 50% increment of the corrosion-fatigue strength of the material in saline. Also, the enhanced osteoblast attachment and proliferation were observed on their developed NG-316L SS. They attributed these enhancements to the thicker oxide layer and increased charge carrier density of the n-type oxide film resulting from the NG surface on the 316L SS.[9] Bagherifard et al. also pointed out that the surface topography and grain size of the substrate could affect cell activities. They evaluated the capability of severe shot peening to modulate the interactions of nanocrystalline metallic biomaterials with cells and found a

Received: February 11, 2018
Accepted: March 27, 2018
Published: March 27, 2018

DOI: 10.1021/acsbiomaterials.8b00173
ACS Biomater. Sci. Eng. 2018, 4, 1609−1621

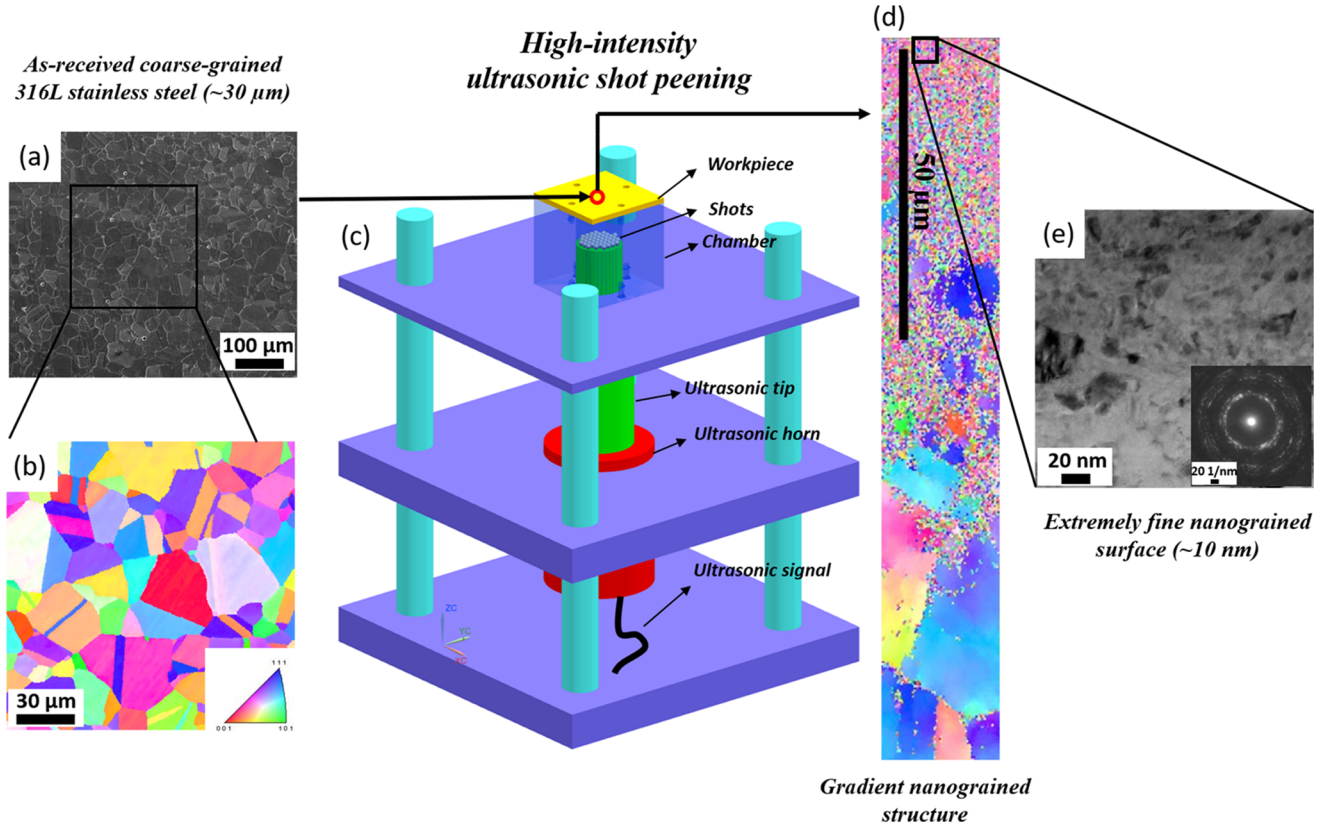

Figure 1. (a) Scanning electron microscopy (SEM) characterization of the as-received CG-316L SS. (b) EBSD characterization of the as-received CG-316L SS. (c) Principle and experimental setup of the USP. (d) Gradient nanograined structure of the USPed 316L SS sample. (e) Extremely fine NG-316L SS characterized by TEM.

significant enhancement in maintenance of osteoblast adhesion and proliferation on the NG-316L SS surface compared to the nontreated coarse-grained 316L SS (CG-316L SS) materials.[10] Nune et al. announced that bulk nanostructured materials are recognized as potential implant materials alternative to conventional materials because of the promoted cellular activities and antimicrobial on the NG surface compared to its CG counterparts.[11] Misra et al. used "phase reversion" plus a controlled deformation-annealing method to obtain a wide regime of grain sizes, starting from the NG regime (320 nm) to the CG regime (22 μ), and demonstrated that the grain size of the metallic surface significantly impacts cellular interaction and osteoblast functions.[12,13] In 2016, Yin et al. reported a novel "net-like" NG cell−substrate metallic surface for human osteoblast cell's function enhancement by increasing the surface energy and surface hydrophilicity via surface nanostructuring of 316L SS.[14] The "in vitro" investigations indicated the enhancement of the osteoblast cell function by using the cell−substrate in a nanosized grain structure. It should be mentioned that the average grain size of the developed "net-like" NG cell−substrate metallic surface is around 200 nm, which is the same order of magnitude as the previously published NG/UFG materials.[10,15,16]

The application of a finer grain-structured cell−substrate interface was reported by Huo et al. in 2017. A nanocrystalline surface with an average grain size smaller than 20 nm was fabricated on tantalum via sliding friction treatment (SFT). They pointed out that higher surface hydrophilicity, enhanced corrosion resistance, and higher percentage of protein adsorption were identified on the NG surface than those on the CG surface.[17] It was also stated that the adsorption of proteins on metallic surfaces is nonspecific and preferentially occurs along the higher energy regions such as the second phase particles and grain boundaries, which could provide a continuum of probable binding sites with partial surface coverage.[11,18,19] Hence, the finer NG surface, which has higher grain boundary density, will have higher surface energy and more protein adsorption binding sites when the materials encounter biological environments compared to its CG or UFG counterparts. Meanwhile, grain boundary can also be an obstacle to the dislocation movement when the material undergoes plastic deformation, which can be used for the mechanical strengthening of the biometallic materials.[20,21] It was expected that the yield strength of this NG surface layer will be pretty high according to the classic "Hall−Petch equation"[22,23] shown as follows:

$$\sigma_y = \sigma_0 + k_1 D_{GB}^{-1/2} \quad (1)$$

where σ_y is the yield stress, σ_0 and k_1 are the constants, σ_0 is a friction stress, and D_{GB} is the grain size of the material. The improved hardness and yield strength will potentially benefit the wear resistance and fatigue life of the bioimplant metallic devices.[24−26]

On the basis of the hypothesis demonstrated above, a finer NG surface will provide better mechanical and biological performance when used as bioimplant materials. Furthermore, the rough surface generated by ultrasonic shot peening (USP) can also benefit the human osteoblast cell's functions according to the previously published literature.[27−31] These two characteristics make the proposed extremely fine NG rough

DOI: 10.1021/acsbiomaterials.8b00173
ACS Biomater. Sci. Eng. 2018, 4, 1609−1621

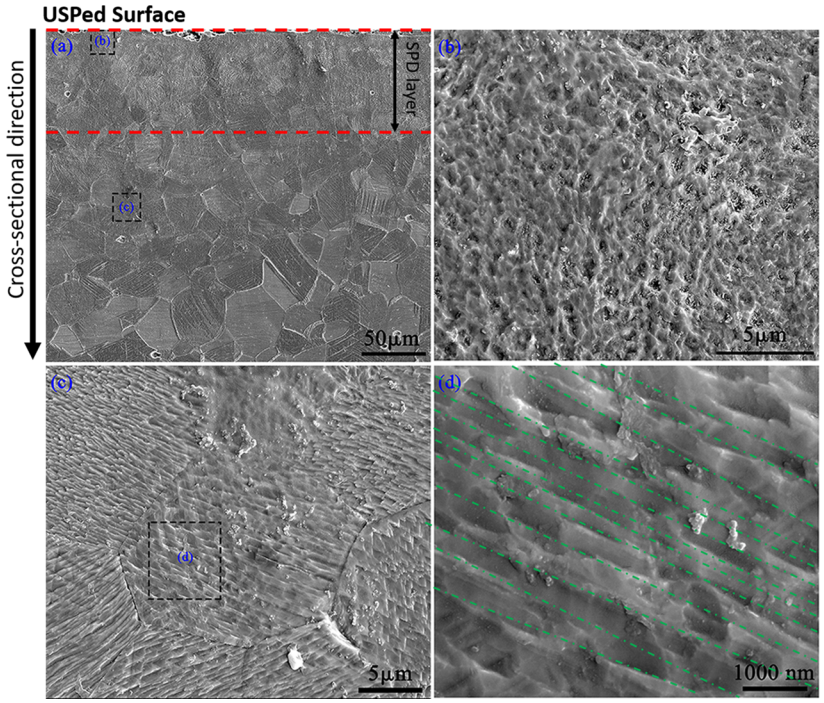

Figure 2. (a) Cross-sectional characterization of the NG-316L SS with a peening time of 600 s. (b) Microstructure of the NG-316L SS with severe deformation at the topmost surface. (c) Microstructure of the NG-316L SS fabricated at a depth of around 150 μm. (d) Magnified characterization of the NG-316L SS structure with the average grain thickness/size of 300 nm.

materials an ideal candidate for the advanced load-bearing biomedical materials.

However, the application of the NG rough 316L SS surface with the average grain size that is roughly 10 nm fabricated by USP in strengthening the mechanical performance of the bioimplant materials and modulating the human osteoblast cell's functions has not been reported yet. In this study, we report a strategy that could enhance the mechanical and biological performance of 316L SS in orthopedic applications by generating the rough surface and extremely fine nanosized grains via USP simultaneously. The extremely fine NG rough surface with the average grain size of 10 nm was successfully fabricated. This extremely fine NG rough surface was proposed to be used as the advanced cell−substrate interface to enhance the mechanical and biological performance of the bioimplant materials. In addition, the extremely fine NG rough surface layer that was "coated" on the materials will increase the mechanical performance of the entire components as well.[32,33] Nanoindentation tests and micropillar compression tests are conducted to reveal the nanohardness and yield strength of the NG-316L SS surface, respectively. Macroscale and microscale roughness of the NG-316L SS and CG-316L SS surface is measured by a noncontact profilometer. The effect of the extremely fine NG-316L SS rough surface on the attachment of the human osteoblast cells at the early stage is investigated and discussed.

2. MATERIALS AND METHODS

2.1. Materials and Ultrasonic Shot Peening. The commercially available 316L SS sheet with the thickness of 3 mm was purchased from the OnlineMetals (USA). All the samples were cut into small pieces with a dimension of 50 × 50 mm^2 to fit our USP facility. The microstructure of the as-received CG- 316L SS with an average grain size of 25 μm was characterized by using the scanning electron microscope (SEM) as illustrated in Figure 1a. The principle of USP, which was used to fabricate the extremely fine NG rough surface on 316L SS,[14,34,35] was illustrated in Figure 1c. Fifty high-strength chrome steel shots with the dimeter of 3 mm were used. The working distance H, which is defined as the distance from the materials to the ultrasonic vibrating surface, is 10 mm. The peening duration to get the extremely fine NG-316L SS used in this study is 10 min. The frequency of the ultrasonic signal is 20 kHz. Detailed setup of the USP can be found in our previously published papers.[14,34,36−39] It should be noted that the chamber is made from 316L SS to avoid the surface containment. Figure 1b and Figure 1d show the EBSD characterizations of the 316L SS before and after USP, respectively. CG-316L SS surface was refined into NG structure after USP according to Figure 1b and Figure 1d. And the extremely fine NG surface fabricated at the topmost surface of the 316L SS sample was characterized by using TEM and illustrated in Figure 1e.

2.2. Materials Characterizations. The FEI QUANTA 3D FEG scanning electron microscope (SEM) equipped with electron beam and ion beam was used to characterize the microstructure of the NG-316L SS. Before the SEM characterization, the cross-sectional 316L SS sample was mechanically polished and then etched at room temperature in a solution of the mixture of hydrochloric acid, nitric acid, and distilled water with a volume ratio of 1:1:1. Finer structure of the NG-316L SS surface was characterized via focused ion beam (FIB) channeling contrast image technique,[40−42] and transmission electron microscope (TEM) was utilized to give the quantified distribution of the nanosized grains. The TEM sample was prepared by the FIB lift-out method by using the FEI QUANTA 3D FEG SEM equipped with the Omniprobe AutoProbe 200 lift-out system. The bright-field (BF), dark-field (DF) images and the selected area diffraction (SAD) pattern of the NG-316L SS were captured by using an FEI Tecnai G20 TEM. A EBSD detector was employed to characterize the grain orientation of the as-received CG-316L SS and NG-316L SS after USP. Grain size distribution was analyzed and plotted by using the MATLAB. Chemical compositions of the aggregated particles on the NG rough 316L SS surface are analyzed by using an Oxford EDX detector.

2.3. Mechanical Tests. *2.3.1. Nanohardness.* Nanohardness measurements were performed on the USPed sample along the cross-sectional direction from the peened surface to the matrix

DOI: 10.1021/acsbiomaterials.8b00173
ACS Biomater. Sci. Eng. 2018, 4, 1609−1621

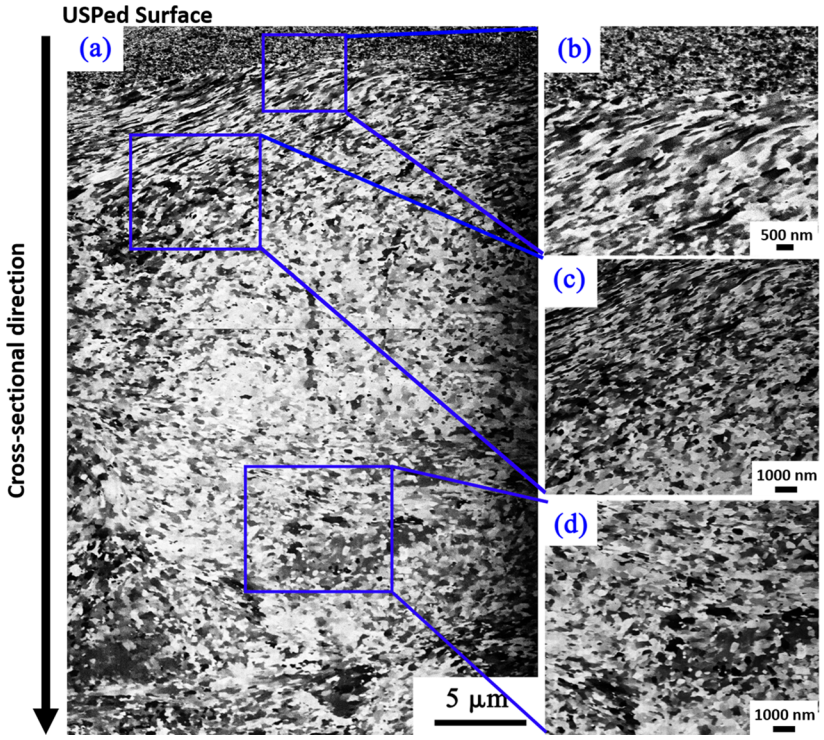

Figure 3. (a) Focused ion beam channeling contrast image for the cross-sectional characterization of the USPed 316L SS after 600 s treatment and the microstructure of the USPed 316L SS at (b) the topmost surface with an extremely fine NG surface and (c) 15 μm and (d) 30 μm depth from the topmost surface.

materials by using the Agilent Technologies Nanoindenter G200. Standard Oliver and Pharr method[43] was used to get the nanohardness and elastic modulus of the materials from the force-displacement curves. Indentations with maximum depth of 500 nm were conducted. The loading, holding, and unloading times were 20, 5, and 20 s, respectively. 200 indents along the cross-sectional direction on the sample were conducted where the spacing between the first 100 indents was set as 2 μm and the spacing between the second 100 indents was set as 5 μm. For a Berkovich indenter, the spacing of 2 μm is large enough to eliminate the influence from neighboring indents.

2.3.2. Micropillar Compression. FIB was utilized to fabricate micropillars with the diameter of ~3 μm and height of ~6 μm on the NG-316L SS and CG-316L SS. Two micropillars were fabricated at the location of 5 and 1500 μm depth from the peening surface. To guarantee the surface quality of the pillars, the current of the final polish is 0.1 nA. Micropillar compression experiment was conducted on the AGILENT Technologies Nanoindenter G200 with a flat diamond tip. The geometry of the flat tip can be seen in the Figure 6e. The entire displacement of the tip is 2000 nm with the strain rate of 0.01 s^{-1}.

2.4. Surface Conditions. Surface roughness of the 316L SS before and after USP was measured by using the Contour GT-K optical profiling system (Bruker Nano, Inc.). Measurements at five different locations with the scanning area of 2271.76 × 1703.82 μm^2 were used to study the macroscale surface roughness of the CG-316L SS and NG-316L SS surface. To get the microscale surface roughness of the CG-316L SS and NG-316L SS surface, higher magnification (100×) measurements with the corresponded scan areas of 62.96 × 42.22 μm^2 were conducted. X-ray diffraction (XRD) was performed by using the Bruker D8 focus X-ray diffractometer to identify the constituent phases of the 316L SS before and after USP. XRD profiles were recorded by using Cu Kα radiation with a scan speed of 10°/min and an angular step of 2θ = 0.02°. The raw XRD test data without filtering were directly illustrated.

2.5. Cell Experiments. *2.5.1. Cell Line and Culture Medium.* The cell line used in this study is the Saos-2 (ATCC HTB-85) human osteoblast cell purchased from the ATCC, USA. A phenol-free osteoblast basal medium with 1% penicillin/streptomycin and an osteoblast supplemental mix (McCoy's 5A Medium, ATCC) was used as the cell culture medium. The cells were cultured in a 37 °C, humidified 5% CO_2/95% air environment.

2.5.2. Cell Attachment and Coverage. Saos-2 human osteoblast cells were seeded on the NG-316L SS and CG-316L SS surface with a cell density of 500 000 cells/cm^2. To study the cell attachment and coverage at its early stage, the cells were cultured for 4 h. Then, a 2.5% glutaraldehyde solution in PBS was used to fix the cells for 30 min at 4 °C. And the cells were dehydrated with a graded ethanol series (50%, 70%, 90%, and 100%). After the 100% ethanol step, samples were immersed in the 100% hexamethyldisilazane (HMDS, Sigma) for 3 min and air-dried in a fume hood. An ultrathin platinum conductive layer was coated on the cells by using the Cressington sputter coater. The FEI QUANTA 3D FEG SEM was used to characterize the cell attachment and coverage on the NG-316L SS and CG-316L SS surface. The cell coverage area is defined as the area that is covered by the tissue on the metallic surface and analyzed by the ImageJ.[44]

3. RESULTS

3.1. Nanograined Surface Characterizations. Figure 2 shows the SEM characterizations of the cross-sectional 316L SS after USP with the peening duration of 10 minutes. The peened surface was carefully examined and is free of crack and failure. It can be seen in Figure 2a that the thickness of the severely plastically deformed (SPDed) layer is almost 100 μm. In this area, the grain boundaries cannot be identified clearly. Figure 2b is the magnified observation of the peened 316L SS at the topmost peened surface. The materials at this area were SPDed and the NG structure cannot be characterized via chemical metallographic corrosion method. Figure 2c and Figure 2d are the microstructure of the peened 316L SS at a depth of 150 μm. It can be seen in Figure 2c and Figure 2d that the materials at this depth were refined into "net-like" nanostructure with an

DOI: 10.1021/acsbiomaterials.8b00173
ACS Biomater. Sci. Eng. 2018, 4, 1609−1621

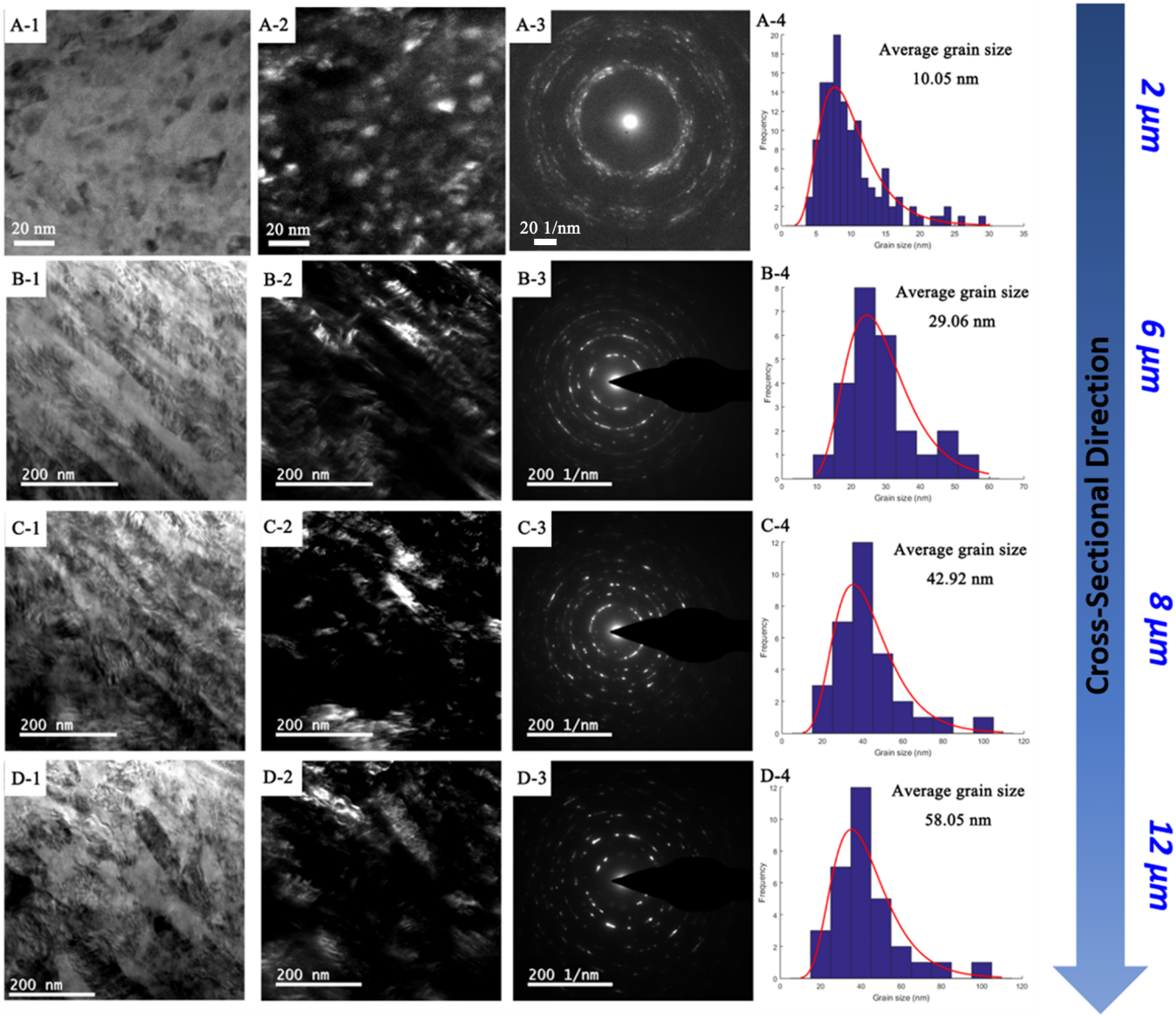

Figure 4. (A-1) Bright field (BF) and (A-2) dark field (DF) TEM observations of the NG-316L SS at the location of 2 μm depth from the peened surface; (A-3) diffraction pattern of the corresponding area and (A-4) the grain size distribution of this material with an average grain structure of 10.05 nm; (B-1) BF and (B-2) DF TEM observations of the NG-316L SS at the location of 6 μm depth from the peened surface; (B-3) diffraction pattern of the corresponding area and (B-4) the grain size distribution of this materials with an average grain structure of 29.06 nm; (C-1) BF and (C-2) DF TEM observations of the NG-316L SS at the location of 8 μm depth from the peened surface and (C-3) the diffraction pattern of the corresponding area and (C-4) the grain size distribution of the materials with an average grain structure of 42.92 nm; (D-1) BF and (D-2) DF TEM observations of the NG-316L SS at the location of 12 μm depth from the peened surface and (D-3) the diffraction pattern of the corresponding area and (D-4) the grain size distribution of the materials with an average grain structure of 58.05 nm.

average grain thickness of 300 nm, which is similar to the structure obtained in the authors' previous research.[14]

The SPDed surface layer as shown in the Figure 2a was characterized by using the FIB channeling contrast imaging technique. Figure 3 shows the FIB channeling contrast images of the NG-316L SS from the view of cross-sectional direction at the SPDed layer. Figure 3b shows the magnified observation of the microstructure at the topmost peened surface layer. The average grain size and the thickness of the extremely fine NG surface layer are 10 nm and 2 μm, respectively. This extremely fine NG surface will be used as the cell−substrate interface for the biological enhancement of bioimplant materials in orthopedic applications. Figure 3c illustrates the microstructure of the USPed sample at the location of 15 μm depth from the peened surface. The grain size at this location is bigger than that at the topmost surface as characterized in the Figure 3 b, and with the increase of the distance from the peened surface, the grain size increases gradually from tens of nanometers to hundreds of nanometers. Figure 3 d shows the microstructure of the USPed sample at the location of 30 μm depth from the peened surface. At this region, the grains have been refined into hundreds of nanometers.

To get the quantified characterization of the NG surface fabricated by USP, a TEM lamellar was prepared at the top surface by the SEM-FIB system and characterized by the TEM. Figure 4 illustrates the TEM characterizations and the grain size distribution of the fabricated NG-316L SS at locations of 2, 6, 8, and 10 μm depth from the peening surface. It can be seen in

DOI: 10.1021/acsbiomaterials.8b00173
ACS Biomater. Sci. Eng. 2018, 4, 1609−1621

parts A-1 and A-2 of Figure 4 that extremely fine NG structure was fabricated in this surface layer. Figure 4A-3 shows the selected area diffraction (SAD) pattern of the NG materials of this surface layer. The grain size distribution of this layer is depicted in Figure 4A-4. The log-normal distribution function was used to fit the grain size distribution, and the average grain size is 10.05 nm of this surface layer. Parts B-1 and B-2 of Figure 4 are the BF and DF TEM observations of the NG-316L SS at the location of 6 μm depth from the peening surface. The grains at this surface layer have been elongated, and there is some tiny grain structure in the lath-shaped grains as well. The average grain size of this materials is 29.06 nm according to the grain size distribution analysis as shown in the Figure 4B-4. Parts C and D of Figure 4 demonstrated the microstructure of the NG-316L SS at surface layers of 8 and 10 μm depth from the peening surface. The average grain size of these two surface layers is 42.92 and 58.05 nm, respectively. It can be seen in Figure 4 that with the increment of the depth of the surface layer, the average grain size increased gradually from 10 nm to almost 60 nm and the appearance of Debye−Scherrer rings changed from "continuous" to "spotty", reflecting the increase in the average grain size from the topmost surface to the deeper surface layer as well.

In summary, the SEM observations indicated that the thickness of the gradient NG surface was almost 100 μm and followed by "net-like" nanostructured materials with the average grain thickness of 200−300 nm. And the FIB channeling image as shown in Figure 3 indicated the gradient NG surface layer with the grain size from several nanometers to hundreds of nanometers was successfully fabricated on the 316L SS. And the TEM characterizations indicated that the average grain size of the developed extremely fine NG surface is 10 nm, following by the NG materials with the average grain size of 29.06, 42.92 and 58.05 nm at the depth of 6, 8, and 12 μm, respectively. Biologically, the extremely fine NG surface layer at top surface will provide numerous binding site for the proteins and be used as the cell−substrate interface to increase the biological performance of the materials in orthopedic applications. Mechanically, the developed thick gradient NG surface layer will greatly increase the mechanical performance such as fatigue life, wear resistance, etc. of the entire bioimplant materials according to the previously published literature.[25,45−48]

3.2. Mechanical Behaviors. *3.2.1. Nanohardness Testing.* Figure 5a shows the nanohardness of the NG-316L SS sample along the cross-sectional direction. It can be seen in Figure 5a that the nanohardness decreases with the increment of the distance from the peened surface. This trend agrees well with the gradually increased nanostructure characterized in section 3.1. The hardest material is located at the peened surface, and the nanohardness is 5.875 GPa. The nanohardness of the matrix materials with CG-316L SS is 3.269 GPa. The nanohardness of the fabricated NG surface layer was increased by up to 79.72%. Figure 5b is the measurement of the modulus of the USPed 316L SS along the cross-sectional direction. There is no notable change of the modulus between the NG-316L SS and CG-316L SS. And the average modulus of the USPed 316L SS is 198.52 GPa.

3.2.2. Yield Strength. The true stress−strain curves of the compression tests were calculated based on the force displacement of the tip according to the classical model proposed by Sneddon.[49] The detailed calculation procedures of the true stress−strain curves can be found in the previously

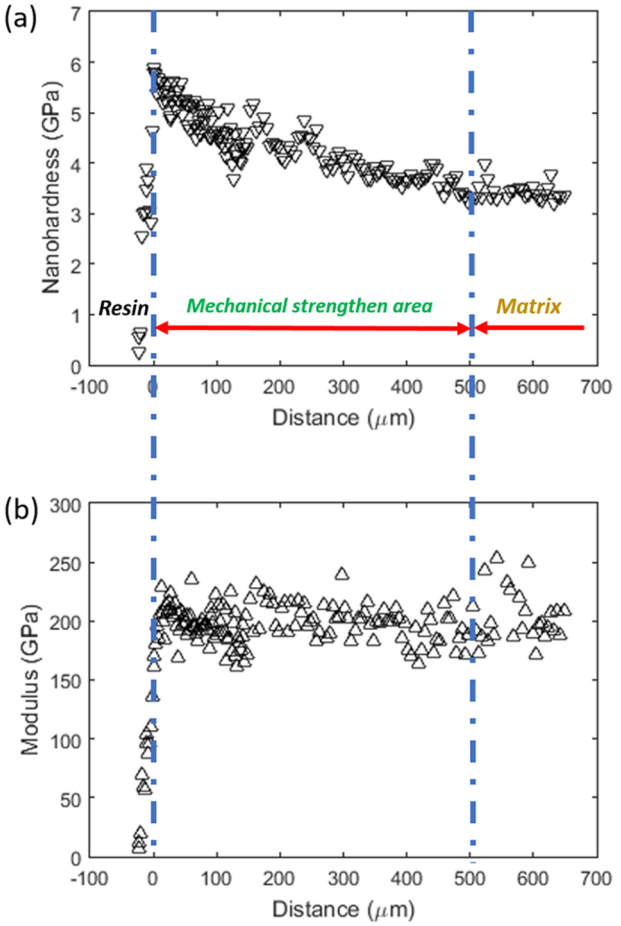

Figure 5. Variation of the (a) nanohardness and (b) Young's modulus of the USPed 316L SS with distance away from the peened surface.

published literature.[50,51] And the true strain (ε) and true stress (σ) are expressed as follows by referring to equations presented by Zhang et al.:[52]

$$\varepsilon = \frac{1}{E_{ss}}\frac{PL_p}{A_0L_0} + \ln\left(\frac{L_0}{L_p}\right) \tag{2}$$

$$\sigma = \frac{P}{A_p} = \frac{PL_p}{A_0L_0} = \frac{P}{A_0L_0}\left\{L_0 - \left[u_{tot} - \frac{\sqrt{\pi}P(1-\nu_{SS}{}^2)}{2E_{sub}\sqrt{A_{sub}}}\right]\right\} \tag{3}$$

where P is the load; L_0 is the half initial height of the pillar; A_0 is the cross-sectional area at half initial height; L_p and A_p are the final height and average cross-sectional area of the pillar, respectively; E_{SS} is the Young's modulus of the 316L SS (~198.52 GPa); and ν_{SS} is Poisson's ratio of the 316L SS (~0.275). Different from the experimental setup of Zhang et al.,[52] the other end of the pillar was on the matrix of the sample in this study. Hence, the modulus (E_{sub}) and average cross-sectional area of the substrate (A_{sub}) are 198.52 GPa and infinity, respectively. u_{tot} is the total displacement of the tip measured by the system according to eq 4.[53]

$$u_{tot} = u_{measured} - \frac{1-\nu_{Dia}{}^2}{E_{Dia}}\left(\frac{P}{D_{top}}\right) - \frac{1-\nu_{Sub}{}^2}{E_{Sub}}\left(\frac{P}{D_{bottom}}\right) \tag{4}$$

DOI: 10.1021/acsbiomaterials.8b00173
ACS Biomater. Sci. Eng. 2018, 4, 1609−1621

where $u_{measured}$ is the displacement of the tip measured by the nanoindenter; E_{Dia}, E_{Sub}, ν_{Dia}, and ν_{Sub} are the modulus and Poisson's ratios of the diamond indenter (1141 GPa and 0.07 [53]) and the substrate of the micropillars. D_{top} and D_{bottom} are the upper and the lower diameters of each micropillar, respectively.

Finally, the true strain and true stress during the micropillar compression tests can be calculated by eqs 5 and 6 by substituting eq 4 into eqs 2 and 3, respectively.

$$\varepsilon = \frac{1}{E_{ss}} \frac{P\left(L_0 - \left(u_{measured} - \frac{1-\nu_{Dia}^2}{E_{Dia}}\left(\frac{P}{D_{top}}\right) - \frac{1-\nu_{Sub}^2}{E_{Sub}}\left(\frac{P}{D_{bottom}}\right)\right)\right)}{A_0 L_0} + \ln\left(\frac{L_0}{\left(L_0 - \left(u_{measured} - \frac{1-\nu_{Dia}^2}{E_{Dia}}\left(\frac{P}{D_{top}}\right) - \frac{1-\nu_{Sub}^2}{E_{Sub}}\left(\frac{P}{D_{bottom}}\right)\right)\right)}\right) \quad (5)$$

$$\sigma = \frac{P}{A_0 L_0}\left\{L_0 - u_{measured} + \frac{1-\nu_{Dia}^2}{E_{Dia}}\left(\frac{P}{D_{top}}\right) + \frac{1-\nu_{Sub}^2}{E_{Sub}}\left(\frac{P}{D_{bottom}}\right)\right\} \quad (6)$$

where L_0, A_0, D_{top}, D_{bottom} can be measured before micropillar compression test; P and $u_{measured}$ can be obtained from the nanoindentation during the micropillar compression tests.

Figure 6 illustrates the true stress–strain curves of the micropillars fabricated on the USPed sample at the locations of

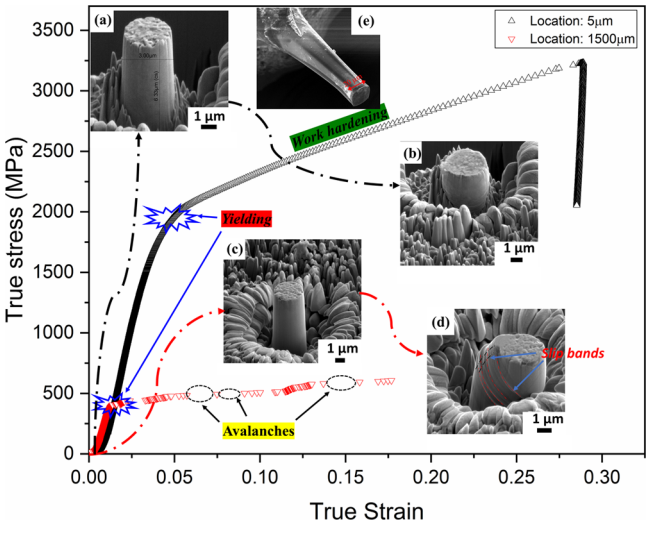

Figure 6. True stress–strain curves of the NG and CG micropillar obtained from the micropillar compression tests and the microstructure of the (a, b) NG and (c, d) CG micropillar before and after compression (the images were captured with a 52° tilt of the specimens in SEM) and (e) the flat tip used for micropillar compression tests.

5 and 1500 μm depth. The stress–strain curve for the NG micropillar is smooth, and the flow stress includes an elastic region and work hardening region. For the true stress–strain curve of the CG micropillar as shown in the Figure 6, there are some visible strain avalanches as indicated in Figure 6. The strain avalanche is a well-known phenomenon characterizing the plasticity of micropillars of single crystals, where complex dislocation processes take place intermittently causing scale-free isolated slip events.[54] The yield strength of the micropillar at the location of 5 μm depth is 1.91 GPa and the yield strength of the micropillar at the location of 1500 μm depth is only 0.39 GPa, which indicated significant yield strength enhancement at the NG surface layer. The microstructures of the NG and CG micropillar before and after compression tests were characterized in Figure 6a,b and Figure 6c,d, respectively. It can be seen in Figure 6b that there is no obviously observed slip bands of the deformed pillar. For the micropillar fabricated from the CG materials, dislocation movements dominate during the plastic deformation of the micropillar.[55] Obvious slip bands were characterized on the surface of the deformed CG pillar as shown in Figure 6d.

3.3. Surface Conditions. Figure 7a illustrates the macroscale surface topography of the 316L SS after USP. The entire scan area is 2272 × 1740 μm^2. It can be seen in Figure 7a that a rough surface was successfully generated by USP and the Ra and Rt of the surface is 2.02 and 19.8 μm, respectively. Rt is the distance between the highest peak and lowest valley on the scanned area. Considering the cell is very tiny, typically tens of micrometers, microscale surface roughness measurements with higher magnification (100×) were performed on the surfaces before and after USP as well. Figure 7b and Figure 7c show the microscale surface roughness of the 316L SS before and after USP. The Ra of the surface before and after USP is 86.27 and 125 nm, respectively. USP can increase the surface roughness of the materials in microscale. According to Deligianni et al.,[27] cell attachment and proliferation are surface roughness sensitive and increased as the roughness of surface increased. Furthermore, it can be seen in the Figure 7b and Figure 7c that the surface topography of the sample before and after USP is totally different. The original polished regular and uniform surface, consisting of parallel grooves, was totally modified into irregular and nonuniform rough surface with microsized peaks. The different surface topography at microscale can affect the human osteoblast cell's functions as well according to the previously published literature.[27,29,31] Figure 7d illustrates the XRD profiles of the 316L SS before and after USP. It can be seen in the XRD profiles that strain induced (110) α phase was identified on the NG rough surface, which agrees with the research results published by Roland et al.[32]

3.4. Human Osteoblast Cell Functions. Figure 8a and Figure 8c show the SEM of the human osteoblast cell (SaoS-2) cultured on the CG-316L SS surface and the extremely fine NG-316L SS surface after 4 h, respectively. The cell coverage area and the cell density on the NG-316L SS surface are greater than those on the CG-316 SS surface. Figure 8e and Figure 8f are the statistical analysis of the cell density and cell coverage of the human osteoblast cell (SaoS-2) cultured on CG-316L SS surface and NG-316L SS surface after 4 h, respectively. The statistical analysis indicted significant difference of the cell coverage area and cell density on the CG-316L SS surface and the NG-316L SS surface. Figure 8b and Figure 8d are the magnified observation of the areas indicated in Figure 8a and Figure 8c, respectively. The morphology of the cell cultured on the CG-316L SS surface and NG-316L SS surface is different. The round characteristic shape of the human osteoblast cell morphology was observed on the NG-316L SS surface as indicated by the red dash line in Figure 8d. This finding is similar to the finding that round characteristic shape of the

DOI: 10.1021/acsbiomaterials.8b00173
ACS Biomater. Sci. Eng. 2018, 4, 1609–1621

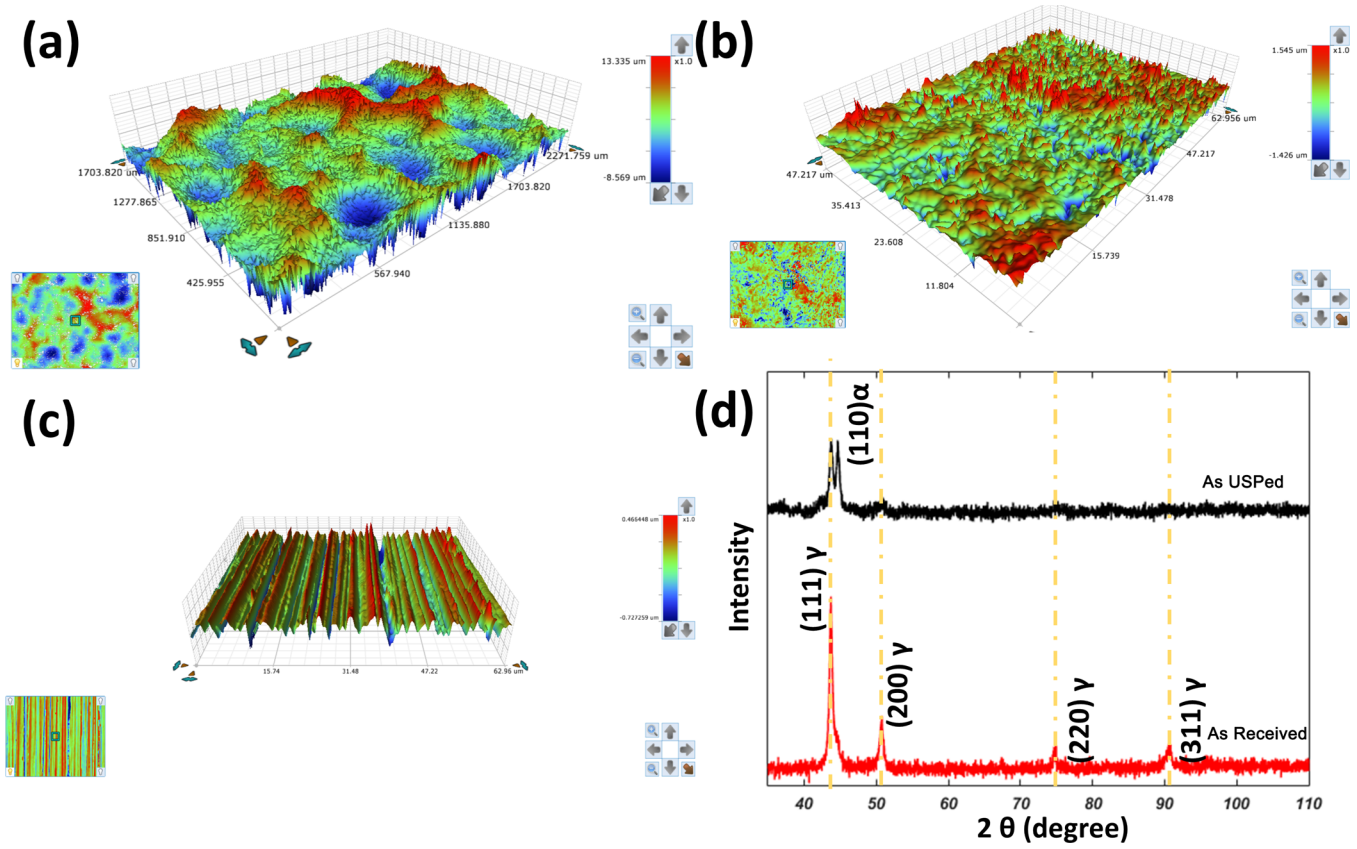

Figure 7. (a) Macroscale surface topography of the NG-316L SS surface and the microscale surface roughness of the NG-316L SS (b) after and (c) before USP. (d) XRD profiles of the as-received CG-316L SS and the NG-316L SS (γ, austenite; α, martensite).

chondrocytes can be observed on the TiO_2 nanotubes with a diameter of less than 100 nm.[56] The research results indicated that the proposed extremely fine NG rough 316L SS surface could modulate the attachment and shape of the human osteoblast cells.

4. DISCUSSION

In this study, a gradient NG surface layer with the microstructure from tens of nanometers to hundreds of nanometers was successfully fabricated on the 316L SS and the extremely fine NG surface with the average grain structure of 10 nm was used as the cell−substrate interface for mechanical and biological enhancement of bioimplant materials in orthopedic applications. The materials characterization results as shown in Figures 2−4 demonstrated that a gradient NG surface layer with the thickness of 100 μm has been successfully generated on the 316L SS sample and an extremely fine NG surface layer with the average grain structure of 10 nm and thickness of 2−4 μm was developed at the topmost peened surface. In Figure 2c and Figure 2d, the multiple-slip and microbands structures were characterized in the NG-316L SS sample, and these features are similar to the microstructures demonstrated in Figure 1a and Figure 1c of ref 57. And the randomly orientated extremely fine nanograins with the average grain size of 10 nm as shown in Figure 3b and Figure 4A were generated on the 316L SS in this study.

Figure 5 demonstrated the nanohardness and Young's modulus of the gradient NG surfaces generated in the NG-316L SS sample. The nanohardness measurements and the microstructure characterizations suggested that the influence of USP on the mechanical properties of the 316L SS can penetrate to the depth of around 500 μm. However, according to the materials characterization as shown in the Figure 2, the thickness of the gradient NG/UFG surface layer is around 150 μm. A similar phenomenon was reported by Bagherifard et al.[10] They used severely shot peening method to obtained nanograined surface layer on the 316L SS. A surface nanocrystallization layer with a thickness of 150−200 μm was successfully fabricated. However, the thickness of the mechanical enhanced surface layer is roughly 800 μm. The profile of the residual stress distribution in that study indicated that the thickness of the compressive residuals stress layer is almost 700 μm. Compared to the research results reported by Bagherifard et al., we believe that the thickness of the surface layer with the compressive residual stress in our study could be 600−700 μm. That is also the reason why the thickness of the mechanical enhanced surface layer is thicker than that of the NG/UFG surface layer in our study. Hence, two kinds of mechanical strengthen mechanism could be utilized in this study. The first one is the grain refinement, and the second one is the compressive residual stresses induced by USP.[58] Grain refinement could increase the grain boundary density in the materials, which will obstruct dislocation movement when the materials undergo plastic deformation. The grain refinement mechanism dominates at the region from the peened surface to a depth of around 150 μm based on the microstructure characterization as shown in Figure 2. With the increment of the depth from the peened surface, the microstructure increases to the CG structure gradually, and the compressive residual stress strengthen mechanism was supposed to contribute in the following area.

DOI: 10.1021/acsbiomaterials.8b00173
ACS Biomater. Sci. Eng. 2018, 4, 1609−1621

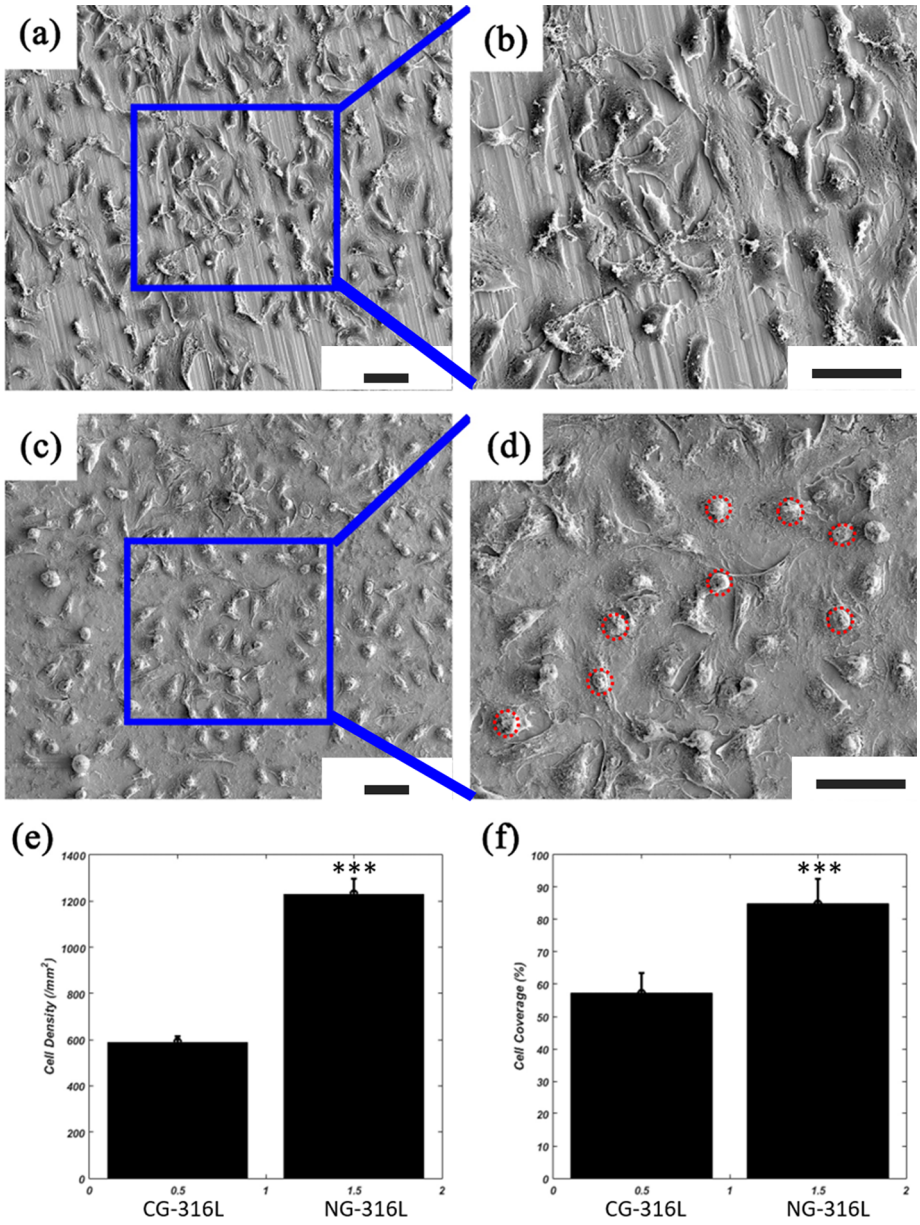

Figure 8. (a) SEM characterization of the human osteoblast cells after 4 h culturing on the CG-316L SS surface and (b) magnified observation of the cell morphology; (c) SEM characterization of the human osteoblast cells after 4 h culturing on the extremely fine NG-316L SS surface and (d) magnified observation showing the round characteristic shape of the human osteoblast cells. Data analysis of the (e) cell density and (f) cell coverage of the human osteoblast cells after 4 h culturing on CG-316L SS surface and NG-316L SS surface. Scale bar is 50 μm. Red dash circles are the selected round characteristic shape of the human osteoblast cells.

To understand the mechanical behavior of the NG surface on the USPed sample, micropillar compression tests were performed on the NG surface layer and CG surface layer. The stress−strain curves can be seen in Figure 6. The stress−strain curve of the NG micropillar is smooth, and there are elastic region and work hardening region. The stress−strain curve of the CG micropillar is disconnected, and there is barely work hardening in the curve. The deformation mechanism in the NG micropillar and CG pillar is different. There are many nanosized grains in the micropillar fabricated from the NG surface layer, while the micropillar fabricated from the CG surface is of single crystalline. The dimension of the pillar is the same. The intrinsic grain size difference makes the deformation mechanism of these two pillars different. Detailed and in-depth investigations to understand the deformation behavior of the NG surface layer fabricated by USP will be conducted in the future.

Furthermore, Chen et al. reported that the yield strength of the nanocrystalline 316L SS with the average grain structure of 40 nm can reach 1.45 GPa.[59] In our study, the nanocrystalline micropillar was fabricated at the location of 5 μm depth from the peening surface. The average grain structure in the micropillar is about 25 nm according to the materials characterization as shown in the Figure 4. The grain size should refer to the grain diameter. Some elongated grain structure is characterized in Figure 4. The thickness of the grains (intercept length) was used as grain size at that surface layer. The yield strength of the nanocrystalline micropillar is 1.91 GPa. The ultrahigh yield strength of this nanocrystalline 316L SS is attributed to the grain size effect in terms of the

DOI: 10.1021/acsbiomaterials.8b00173
ACS Biomater. Sci. Eng. 2018, 4, 1609−1621

Hall–Petch relation. Figure 9 shows a Hall–Petch fitted plot using the data of nanocrystalline 316L SS reported in the previously published literature.[59−62]

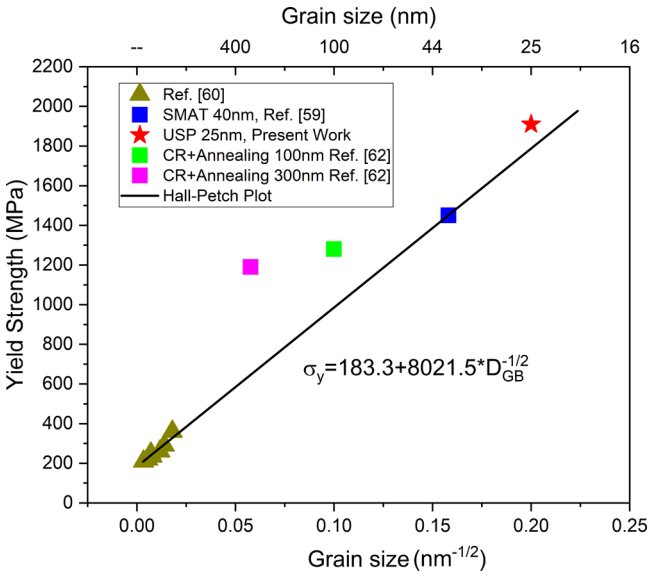

Figure 9. Hall–Petch relationship of the 316L SS plotted by using the data reported in the previously published literature and in this work.

The Hall–Petch relation has been determined to be σ_y = 183.3 + 8021.5$D_{GB}^{-1/2}$ by using the data listed in the published literatures. It is evident that the yield strength of the USPed 316L SS approximately resides on the fitted curve in Figure 9, indicative of lack of softening due to boundary migration-induced grain coarsening. The solutes and precipitates are expected to make pinning effects so as to stabilize the grain boundaries. Note that micropillars in this study have an average diameter of ∼3 μm, which led to negligible "size effect" that has taken place in single and CG crystals. The abundant boundaries that originated from dislocation cell structures during USP process as well as high density dislocation tangles within grain interiors greatly strengthen the USPed materials. The strain hardening in compression experiments at higher stain level is ascribed to dislocation interactions, and the occurrence of dislocation cross-slip might leave extra room for hardening. It should be noted that the compress experiments in the study were not employed to equate with tensile experiments and the yield strength was selected on Hall–Petch plot to compare with existing counterparts.

Figure 7 illustrates the different surface conditions of the 316L SS before and after USP. The macroscale rough surface on the NG 316L SS surface will increase the effective cell attaching area, and the microsized peaks distributed on the NG-316L SS surface will modulate the human osteoblast cell's functions. Surface roughness and topography could play roles in modulating human osteoblast cell's functions. Hence, USP can not only modify the grain structure but also modify the macroscale and microscale surface roughness of the bioimplant materials for the mechanical and biological enhancement of the load-bearing bioimplant materials. Typically, the γ phase in 316L SS is stable because of the presence of molybdenum and it is not prone to martensite formation;[32] however, the mixed α and γ phases are identified on the USPed surface in this study. The α phase should also contribute to the nanohardness increment of the NG-316L SS.

Figure 8 indicated the enhanced attachment and increased cell coverage area of the human osteoblast cells on the extremely fine NG-316L SS surface. It should be noted that the

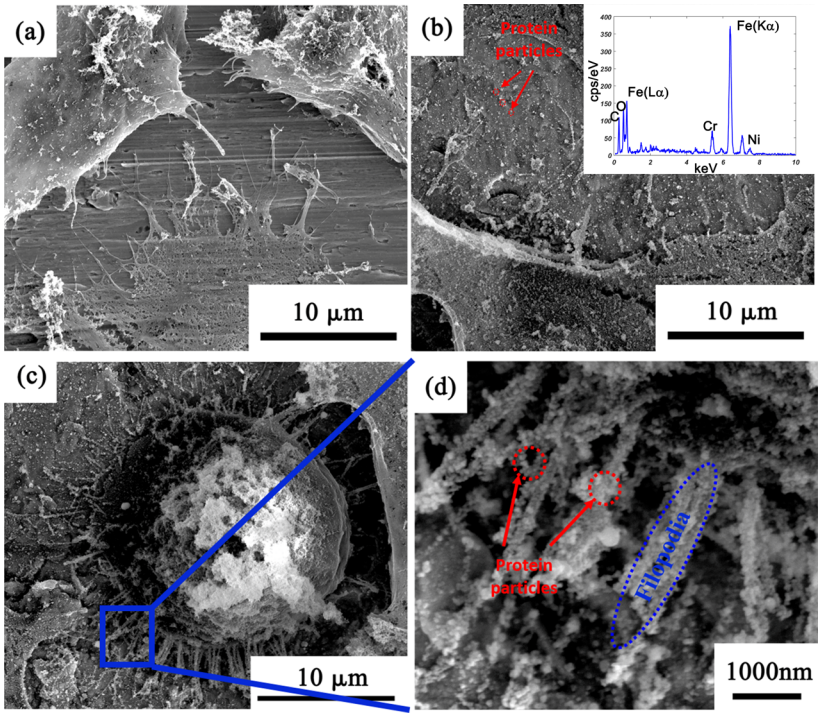

Figure 10. (a) CG-316L SS surface without visible aggregated protein particles and (b) NG-316L SS surface with visible protein particles. The inset is the EDS spectrum of the aggregated particle. (c) Typical human osteoblast cell at the early stage when in contact with the NG-316L SS surface. (d) Observed nanoscale cell filopodia stimulated by the protein particles.

DOI: 10.1021/acsbiomaterials.8b00173
ACS Biomater. Sci. Eng. 2018, 4, 1609−1621

increased cell coverage area may be because of the increased cell number attached on the NG 316L SS rough surface. This biological enhancement could be attributed to the extremely fine NG structure on the peened surface, which could promote protein adsorption. Figure 10a and Figure 10b show the magnified SEM observations demonstrating human osteoblast cell cultured on the CG-316L SS surface and NG-316L SS surface, respectively. There are aggregated protein particles that are evenly distributed on the NG-316L SS surface. However, no aggregated protein particles were observed on the CG-316L SS surface as shown in Figure 10a. The observed aggerated protein particles in Figure 10b are similar to the findings on the TiO_2 nanotubes with the diameter of less than 100 nm developed by Brammer et al.[56] And they pointed out that with the decrement of the diameter of the nanotube, more protein will be adsorbed. The chemical components of the aggregated particle were analyzed by EDS in this study, and the EDS spectrum of the aggregated particle can be seen in the Figure 10b. The carbon and oxygen, which are the essential chemical elements of the protein, are identified in the aggregated particle. It should be noted that the carbon and oxygen are abundant in the environment. The in-depth chemical identification methods for the aggregated protein particles should be performed for future investigations. For instance, Figure 10c shows a typical human osteoblast cell at the early stage when in contact with the NG-316L SS surface. Nanoscale cell filopodia were stimulated by the protein and expanded to attach the substrate surface as shown in the Figure 10d.

In summary, this is the investigation that used extremely fine NG (10 nm) rough surface fabricated by USP for the mechanical and biological enhancement of the 316L SS bioimplant metallic materials. The nanohardness and yield strength of the developed NG-316L SS were tested, and significant mechanical strengthening was achieved. Nevertheless, the previously published literature announced that the increased nanohardness and yield stress of the nanograined surface layer will potentially increase the fatigue life of the mechanical components, the effect of the extremely fine NG surface on the fatigue life of the 316L SS bioimplant materials is still unknown, and the quantified relationship between the grain size and the fatigue life of the materials is needed for precise materials design in the future. The in vitro investigations in this study indicated better attachment and higher coverage area of the human osteoblast cell on the NG-316L SS surface compared to the CG-316L SS surface. Even though the enhanced human osteoblast cell's functions on the NG-316L SS surface can be attributed to the increased protein bonding sites provided by the nanosized grains, the difference of the macroscale and microscale surface roughness between the CG-316L SS surface and NG-316L SS surface can also affect the human osteoblast cell's functions. Furthermore, it should be noted that the compressive residual stress induced into the NG-316L SS could also affect the human osteoblast cell's functions, and we did not perform in-depth investigations on these factors currently. To better understand the effect of the grain size, especially less than 100 nm, surface roughness, and residual stress on the human osteoblast cell's functions, a series of experiments should be conducted in the future and a long-term "in vivo" study should be performed to promote the application of the NG rough surface in bioimplant materials for mechanical and biological enhancement purposes.

5. CONCLUSIONS

In this study, an extremely fine nanograined rough surface with an average grain structure of 10 nm was successfully fabricated on the 316L stainless steel via ultrasonic shot peening, and this extremely fine nanograined rough surface was used as the cell–substrate interface for mechanical and biological enhancements of bioimplant materials in orthopedic applications.

Mechanically, the nanohardness of the developed NG-316L SS surface was increased to 5.875 GPa, which is 79.72% higher than that of the CG-316L SS materials. The yield strength of the NG micropillar fabricated from the surface layer of 5 μm depth is 1.91 GPa, which is 389.74% stronger than that of the CG micropillar fabricated from the surface layer of 1500 μm depth from the peened surface. Furthermore, the thickness of the strengthen area on the USPed 316L SS with the peening duration of 10 minutes is almost 500 μm and the enhanced nanohardness and the yield strength of the thick NG surface layer will potentially increase the wear resistance and fatigue life of the load-bearing bioimplant materials significantly.

Biologically, the extremely fine NG-316L SS rough surface can significantly promote cell attachment and coverage compared with the CG-316L SS surface. Aggregated protein particles were observed on the extremely fine NG surface, which gives firm evidence to confirm that NG surface can promote protein adsorption by providing more probable binding sites with partial surface coverage when material encounters biological environments than its CG counterparts. The enhanced human osteoblast cell's functions on the NG rough surface can be attributed to the increased protein bonding sites provided by the nanosized grains and the increment of the macroscale and microscale surface roughness generated by USP.

In summary, the study demonstrated the use of an extremely fine NG-316L SS cell–substrate interface, with an average grain size of 10 nm, for mechanical and biological enhancement in orthopedic applications. The findings and the surface engineering technology used in this study have the potential to promote the currently proposed concept that using nanostructured cell interface for mechanical and biological enhancement of bioimplant materials in orthopedic applications from the current practice level of "hundreds of nanometers" to that of "tens of nanometers" or possibly even "several nanometers".

AUTHOR INFORMATION

Corresponding Authors

*F.Y.: e-mail, fyin@purdue.edu.

*Q.H.: e-mail, hanq@purdue.edu.

ORCID

Fei Yin: 0000-0002-5897-7477

Author Contributions

The manuscript was written and prepared through contributions of all authors. All authors have given approval to the final version of the manuscript.

Notes

The authors declare no competing financial interest.

ACKNOWLEDGMENTS

This work was supported by the Purdue Center for Materials Processing Research and Center for Technology Development at Purdue University.

DOI: 10.1021/acsbiomaterials.8b00173
ACS Biomater. Sci. Eng. 2018, 4, 1609–1621

ABBREVIATIONS

CG, coarse-grained; NG, nanograined; 316L SS, 316L stainless steel; SEM, scanning electron microscope; FIB, focused ion beam; TEM, transmission electron microscope; EBSD, electron backscatter diffraction; USP, ultrasonic shot peening; SMAT, surface mechanical attrition treatment; SFT, sliding friction treatment; BF, bright field; DF, dark field; SAD, selected area diffraction pattern; CR, cold rolling; EDS, energy-dispersive X-ray spectroscopy

REFERENCES

(1) Nuss, K. M.; von Rechenberg, B. Biocompatibility issues with modern implants in bone—a review for clinical orthopedics. *Open Orthop. J.* **2008**, *2*, 66.

(2) Anselme, K.; Bigerelle, M. Topography effects of pure titanium substrates on human osteoblast long-term adhesion. *Acta Biomater.* **2005**, *1* (2), 211−222.

(3) Anselme, K.; Davidson, P.; Popa, A.; Giazzon, M.; Liley, M.; Ploux, L. The interaction of cells and bacteria with surfaces structured at the nanometre scale. *Acta Biomater.* **2010**, *6* (10), 3824−3846.

(4) Bagherifard, S.; Ghelichi, R.; Khademhosseini, A.; Guagliano, M. Cell Response to Nanocrystallized Metallic Substrates Obtained through Severe Plastic Deformation. *ACS Appl. Mater. Interfaces* **2014**, *6* (11), 7963−7985.

(5) Webster, T. J.; Ergun, C.; Doremus, R. H.; Siegel, R. W.; Bizios, R. Specific proteins mediate enhanced osteoblast adhesion on nanophase ceramics. *J. Biomed. Mater. Res.* **2000**, *51* (3), 475−483.

(6) Bagherifard, S.; Hickey, D. J.; Fintová, S.; Pastorek, F.; Fernandez-Pariente, I.; Bandini, M.; Webster, T. J.; Guagliano, M. Effects of nanofeatures induced by severe shot peening (SSP) on mechanical, corrosion and cytocompatibility properties of magnesium alloy AZ31. *Acta Biomater.* **2018**, *66*, 93−108.

(7) Jang, Y.; Choi, W. T.; Johnson, C. T.; García, A. s. J.; Singh, P. M.; Breedveld, V.; Hess, D. W.; Champion, J. A. Inhibition of Bacterial Adhesion on Nanotextured Stainless Steel 316L by Electrochemical Etching. *ACS Biomater. Sci. Eng.* **2018**, *4* (1), 90−97.

(8) Jindal, S.; Bansal, R.; Singh, B. P.; Pandey, R.; Narayanan, S.; Wani, M. R.; Singh, V. Enhanced osteoblast proliferation and corrosion resistance of commercially pure titanium through surface nanostructuring by ultrasonic shot peening and stress relieving. *Journal of Oral Implantology* **2014**, *40* (S1), 347−355.

(9) Bahl, S.; Shreyas, P.; Trishul, M.; Suwas, S.; Chatterjee, K. Enhancing the mechanical and biological performance of a metallic biomaterial for orthopedic applications through changes in the surface oxide layer by nanocrystalline surface modification. *Nanoscale* **2015**, *7* (17), 7704−7716.

(10) Bagherifard, S.; Hickey, D.; de Luca, A.; Malheiro, V.; Markaki, A.; Guagliano, M.; Webster, T. The influence of nanostructured features on bacterial adhesion and bone cell functions on severely shot peened 316L stainless steel. *Biomaterials* **2015**, *73*, 185−197.

(11) Nune, K.; Misra, R. Biological activity of nanostructured metallic materials for biomedical applications. *Mater. Technol.* **2016**, *31* (13), 772−781.

(12) Misra, R.; Nune, C.; Pesacreta, T.; Somani, M.; Karjalainen, L. Interplay between grain structure and protein adsorption on functional response of osteoblasts: Ultrafine-grained versus coarse-grained substrates. *J. Biomed. Mater. Res., Part A* **2013**, *101* (1), 1−12.

(13) Misra, R.; Nune, C.; Pesacreta, T.; Somani, M.; Karjalainen, L. Understanding the impact of grain structure in austenitic stainless steel from a nanograined regime to a coarse-grained regime on osteoblast functions using a novel metal deformation−annealing sequence. *Acta Biomater.* **2013**, *9* (4), 6245−6258.

(14) Yin, F.; Yang, S.; Hu, S.; Kuang, S.; Han, Q. Enhanced human osteoblast cell functions by "net-like" nanostructured cell-substrate interface in orthopedic applications. *Mater. Lett.* **2017**, *189*, 275−278.

(15) Bagheri, S.; Guagliano, M. Review of shot peening processes to obtain nanocrystalline surfaces in metal alloys. *Surf. Eng.* **2009**, *25* (1), 3−14.

(16) Bagherifard, S.; Ghelichi, R.; Khademhosseini, A.; Guagliano, M. Cell response to nanocrystallized metallic substrates obtained through severe plastic deformation. *ACS Appl. Mater. Interfaces* **2014**, *6* (11), 7963−7985.

(17) Huo, W.; Zhao, L.; Yu, S.; Yu, Z.; Zhang, P.; Zhang, Y. Significantly enhanced osteoblast response to nano-grained pure tantalum. *Sci. Rep.* **2017**, *7*, 40868.

(18) Williams, R.; Williams, D. The spatial resolution of protein adsorption on surfaces of heterogeneous metallic biomaterials. *J. Biomed. Mater. Res.* **1989**, *23* (3), 339−350.

(19) Dufrêne, Y. F.; Marchal, T. G.; Rouxhet, P. G. Influence of substratum surface properties on the organization of adsorbed collagen films: in situ characterization by atomic force microscopy. *Langmuir* **1999**, *15* (8), 2871−2878.

(20) Lu, K.; Lu, L.; Suresh, S. Strengthening materials by engineering coherent internal boundaries at the nanoscale. *Science* **2009**, *324* (5925), 349−352.

(21) Lu, L.; Shen, Y.; Chen, X.; Qian, L.; Lu, K. Ultrahigh strength and high electrical conductivity in copper. *Science* **2004**, *304* (5669), 422−426.

(22) Chokshi, A.; Rosen, A.; Karch, J.; Gleiter, H. On the validity of the Hall-Petch relationship in nanocrystalline materials. *Scr. Metall.* **1989**, *23* (10), 1679−1683.

(23) Hansen, N. Hall−Petch relation and boundary strengthening. *Scr. Mater.* **2004**, *51* (8), 801−806.

(24) Roland, T.; Retraint, D.; Lu, K.; Lu, J. Fatigue life improvement through surface nanostructuring of stainless steel by means of surface mechanical attrition treatment. *Scr. Mater.* **2006**, *54* (11), 1949−1954.

(25) Zhou, L.; Liu, G.; Han, Z.; Lu, K. Grain size effect on wear resistance of a nanostructured AISI52100 steel. *Scr. Mater.* **2008**, *58* (6), 445−448.

(26) Schuh, C.; Nieh, T.; Yamasaki, T. Hall−Petch breakdown manifested in abrasive wear resistance of nanocrystalline nickel. *Scr. Mater.* **2002**, *46* (10), 735−740.

(27) Deligianni, D. D.; Katsala, N.; Ladas, S.; Sotiropoulou, D.; Amedee, J.; Missirlis, Y. Effect of surface roughness of the titanium alloy Ti−6Al−4V on human bone marrow cell response and on protein adsorption. *Biomaterials* **2001**, *22* (11), 1241−1251.

(28) Gittens, R. A.; McLachlan, T.; Olivares-Navarrete, R.; Cai, Y.; Berner, S.; Tannenbaum, R.; Schwartz, Z.; Sandhage, K. H.; Boyan, B. D. The effects of combined micron-/submicron-scale surface roughness and nanoscale features on cell proliferation and differentiation. *Biomaterials* **2011**, *32* (13), 3395−3403.

(29) Rosales-Leal, J.; Rodríguez-Valverde, M.; Mazzaglia, G.; Ramón-Torregrosa, P.; Diaz-Rodriguez, L.; Garcia-Martinez, O.; Vallecillo-Capilla, M.; Ruiz, C.; Cabrerizo-Vílchez, M. Effect of roughness, wettability and morphology of engineered titanium surfaces on osteoblast-like cell adhesion. *Colloids Surf., A* **2010**, *365* (1−3), 222−229.

(30) Marinucci, L.; Balloni, S.; Becchetti, E.; Belcastro, S.; Guerra, M.; Calvitti, M.; Lull, C.; Calvi, E. M.; Locci, P. Effect of titanium surface roughness on human osteoblast proliferation and gene expression in vitro. *Int. J. Oral Maxillofac. Implants* **2006**, *21* (5), 719−725.

(31) Martin, J.; Schwartz, Z.; Hummert, T.; Schraub, D.; Simpson, J.; Lankford, J.; Dean, D.; Cochran, D.; Boyan, B. Effect of titanium surface roughness on proliferation, differentiation, and protein synthesis of human osteoblast-like cells (MG63). *J. Biomed. Mater. Res.* **1995**, *29* (3), 389−401.

(32) Roland, T.; Retraint, D.; Lu, K.; Lu, J. Enhanced mechanical behavior of a nanocrystallised stainless steel and its thermal stability. *Mater. Sci. Eng., A* **2007**, *445*, 281−288.

(33) Wu, X.; Yang, M.; Yuan, F.; Chen, L.; Zhu, Y. Combining gradient structure and TRIP effect to produce austenite stainless steel with high strength and ductility. *Acta Mater.* **2016**, *112*, 337−346.

DOI: 10.1021/acsbiomaterials.8b00173
ACS Biomater. Sci. Eng. 2018, 4, 1609−1621

(34) Yin, F.; Hua, L.; Wang, X.; Rakita, M.; Han, Q. Numerical modelling and experimental approach for surface morphology evaluation during ultrasonic shot peening. *Comput. Mater. Sci.* **2014**, *92*, 28−35.
(35) Yin, F.; Han, Q.; Rakita, M.; Wang, M.; Hua, L.; Wang, C. Numerical modelling and experimental approach for shot velocity evaluation during ultrasonic shot peening. *Int. J. Comput. Mater. Sci. Surf. Eng.* **2015**, *6* (2), 97−110.
(36) Han, Q. Ultrasonic Processing of Materials. *Metall. Mater. Trans. B* **2015**, *46* (4), 1603−1614.
(37) Rakita, M.; Wang, M.; Han, Q.; Liu, Y.; Yin, F. Ultrasonic shot peening. *Int. J. Comput. Mater. Sci. Surf. Eng.* **2013**, *5* (3), 189−209.
(38) Yin, F.; Hu, S.; Hua, L.; Wang, X.; Suslov, S.; Han, Q. Surface Nanocrystallization and Numerical Modeling of Low Carbon Steel by Means of Ultrasonic Shot Peening. *Metall. Mater. Trans. A* **2015**, *46* (3), 1253−1261.
(39) Yin, F.; Rakita, M.; Hu, S.; Han, Q. Overview of ultrasonic shot peening. *Surf. Eng.* **2017**, *33*, 651−666.
(40) Uchic, M.; Groeber, M.; Dimiduk, D.; Simmons, J. 3D microstructural characterization of nickel superalloys via serial-sectioning using a dual beam FIB-SEM. *Scr. Mater.* **2006**, *55* (1), 23−28.
(41) Canovic, S.; Jonsson, T.; Halvarsson, M. Grain contrast imaging in FIB and SEM. *J. Phys.: Conf. Ser.* **2008**, *126*, 012054.
(42) Phaneuf, M. Applications of focused ion beam microscopy to materials science specimens. *Micron* **1999**, *30* (3), 277−288.
(43) Oliver, W. C.; Pharr, G. M. An improved technique for determining hardness and elastic modulus using load and displacement sensing indentation experiments. *J. Mater. Res.* **1992**, *7* (06), 1564−1583.
(44) Grishagin, I. Automatic cell counting with ImageJ. *Anal. Biochem.* **2015**, *473*, 63−65.
(45) Huang, H.; Wang, Z.; Lu, J.; Lu, K. Fatigue behaviors of AISI 316L stainless steel with a gradient nanostructured surface layer. *Acta Mater.* **2015**, *87*, 150−160.
(46) Fang, T.; Li, W.; Tao, N.; Lu, K. Revealing extraordinary intrinsic tensile plasticity in gradient nano-grained copper. *Science* **2011**, *331* (6024), 1587−1590.
(47) Chen, X.; Lu, L.; Lu, K. Grain size dependence of tensile properties in ultrafine-grained Cu with nanoscale twins. *Scr. Mater.* **2011**, *64* (4), 311−314.
(48) Yang, L.; Tao, N.; Lu, K.; Lu, L. Enhanced fatigue resistance of Cu with a gradient nanograined surface layer. *Scr. Mater.* **2013**, *68* (10), 801−804.
(49) Sneddon, I. N. The relation between load and penetration in the axisymmetric Boussinesq problem for a punch of arbitrary profile. *Int. J. Eng. Sci.* **1965**, *3* (1), 47−57.
(50) Bharathula, A.; Lee, S.-W.; Wright, W. J.; Flores, K. M. Compression testing of metallic glass at small length scales: Effects on deformation mode and stability. *Acta Mater.* **2010**, *58* (17), 5789−5796.
(51) Greer, J. R.; Oliver, W. C.; Nix, W. D. Size dependence of mechanical properties of gold at the micron scale in the absence of strain gradients. *Acta Mater.* **2005**, *53* (6), 1821−1830.
(52) Zhang, J.; Liu, G.; Sun, J. Strain rate effects on the mechanical response in multi-and single-crystalline Cu micropillars: Grain boundary effects. *Int. J. Plast.* **2013**, *50*, 1−17.
(53) Sun, Z.; Retraint, D.; Guelorget, B.; Waltz, L. Micro-pillar compression tests to characterize the mechanical behavior of a nanocrystalline layer induced by SMAT in a 316L stainless steel. *Mater. Tech.* **2015**, *103* (3), 304.
(54) Chinh, N. Q.; Győri, T.; Valiev, R. Z.; Szommer, P.; Varga, G.; Havancsák, K.; Langdon, T. G. Observations of unique plastic behavior in micro-pillars of an ultrafine-grained alloy. *MRS Commun.* **2012**, *2* (3), 75−78.
(55) Greer, J. R.; De Hosson, J. T. M. Plasticity in small-sized metallic systems: Intrinsic versus extrinsic size effect. *Prog. Mater. Sci.* **2011**, *56* (6), 654−724.
(56) Brammer, K.; Oh, S.; Cobb, C.; Bjursten, L.; van der Heyde, H.; Jin, S. Improved bone-forming functionality on diameter-controlled TiO_2 nanotube surface. *Acta Biomater.* **2009**, *5* (8), 3215−3223.
(57) Liu, G.; Lu, J.; Lu, K. Surface nanocrystallization of 316L stainless steel induced by ultrasonic shot peening. *Mater. Sci. Eng., A* **2000**, *286* (1), 91−95.
(58) Kobayashi, M.; Matsui, T.; Murakami, Y. Mechanism of creation of compressive residual stress by shot peening. *Int. J. Fatigue* **1998**, *20* (5), 351−357.
(59) Chen, X.; Lu, J.; Lu, L.; Lu, K. Tensile properties of a nanocrystalline 316L austenitic stainless steel. *Scr. Mater.* **2005**, *52* (10), 1039−1044.
(60) Kashyap, B.; Tangri, K. On the Hall-Petch relationship and substructural evolution in type 316L stainless steel. *Acta Metall. Mater.* **1995**, *43* (11), 3971−3981.
(61) Eskandari, M.; Najafizadeh, A.; Kermanpur, A. Effect of strain-induced martensite on the formation of nanocrystalline 316L stainless steel after cold rolling and annealing. *Mater. Sci. Eng., A* **2009**, *519* (1), 46−50.
(62) Üçok, İ.; Ando, T.; Grant, N. J. Property enhancement in Type 316L stainless steel by spray forming. *Mater. Sci. Eng., A* **1991**, *133*, 284−287.

DOI: 10.1021/acsbiomaterials.8b00173
ACS Biomater. Sci. Eng. 2018, 4, 1609−1621